

# Improving the Selected Stages of Integrated-Optic Chip Structure Formation and Its Interfacing with Optical Fibers

Maxim E. Belokrylov<sup>1,2</sup>, Andrey A. Kozlov<sup>2</sup>, Pavel V. Karnaushkin<sup>1</sup>, Yuri A. Konstantinov<sup>1</sup>, Roman S. Ponomarev<sup>1,2</sup>, and Artem T. Turov<sup>1,3</sup>

<sup>1</sup> Perm Federal Research Center, Ural Branch, Russian Academy of Sciences, Perm, Russia

<sup>2</sup> Perm State National Research University, Perm, Russia

<sup>3</sup> Perm National Research Polytechnic University, Perm, Russia

Email: yuri.al.konstantinov@ro.ru

**Abstract**—The paper considers experimental technological regimes at different stages of integrated optical chips creation for modern applications: optoelectronics, fiber-optic sensors, microfluidics. The considered experimental regimes demonstrate not only qualitative, but also quantitative efficiency: at the stage of the ridge waveguides formation, there is a possibility of achieving high etching rates of lithium niobate - up to 950 nanometers per minute in fluorine-containing plasma with an increased consumption of plasma gases without forced thermostating of the sample. Using scanning electron microscope, structural changes in the surface have been demonstrated: clustering of surface etching foci, indicating the uniformity of etching at the macro-scale, and changes in the thickness and structure of the near-surface defect layer, indicating the possibility of its complete removal by the plasma-chemical method. The method can be applied both for the manufacturing of ridge waveguides and optical elements based on them, and for microfluidics elements. Then, the efficiency of the waveguides and optical fibers interfacing method has been confirmed with frequency domain reflectometry. The algorithmic details of the interfacing by the modified Newton's method are also described. The modified Newton's method allowed to simplify the alignment process by performing coarse alignment based on reflections from the far end face of the waveguide, speed up the alignment process at fine mode, and fully automate the alignment of the waveguide and optical fiber at any initial displacements. All the proposed technological process modernization leads to the improvement of technological characteristics and the individual stages production time reduction.

**Index Terms**—Channels formation, integrated circuit creation technology, integrated optical chip, optical frequency domain reflectometry, optical interfacing

## I. INTRODUCTION

Integrated optical circuits are widely used in optoelectronics [1], [2]. The operation parameters of the

most important measuring, research and control systems used in particularly critical engineering facilities, vehicles, and infrastructure facilities, as well as in scientific laboratories around the world depend on their stable functioning. As in microcircuits used in microelectronics, in such chips it is necessary to form the internal structure of optical waveguides, which ensures correct propagation, splitting, coupling, modulation and other processes occurring with radiation inside. The processes of waveguide channels formation have been sufficiently well studied and implemented technologically. In particular, such classical methods as Titan in-diffusion [3], [4], Proton Exchange (PE) [4], [5], ridge waveguide formation [6] and laser written waveguides [7].

Titan in-diffusion is one of the most widespread and well-studied technique for waveguides formation in lithium niobate. This technique allows one to preserve the electro-optical properties of  $\text{LiNbO}_3$  and supports light propagation in both TE and TM modes [4]. Recent advances in the development of Ti in-diffusion waveguides are associated with Er [8] and Tm [9] co-doping.

Lithium niobate Proton Exchange (PE) waveguides are also widely known technique. Such waveguides are characterized by the only extraordinary refractive index change what determines their use in tasks where the state of polarization is important [2]. Also, waveguides created using Soft PE, Annealed PE and reverse PE technologies ensures high stability and allows one to preserve electro-optical and nonlinear optical properties of  $\text{LiNbO}_3$  [10].

Advanced technologies for creating waveguides using a femtosecond laser make it possible to create complex three-dimensional waveguide structures without further processing, which may be useful in a number of practical applications [11].

Lithium niobate ridge waveguides can be created by micromechanical processing [12] or plasma etching [13]. Often, ridge waveguides are produced and used within the "lithium niobate on insulator" (LNOI) technology. Ridge waveguides and LNOI technology allow significant expand applications of lithium niobate [14]. Note that often combined methods of fabricating waveguides are used.

---

Manuscript received October 9, 2021; revised December 19, 2021; accepted December 28, 2021.

Corresponding author: Yuri A. Konstantinov (email: yuri.al.konstantinov@ro.ru).

The Unit II study was funded by RFBR, project № 20-32-90186. The Unit III study was funded by state assignment № AAAA-A19-119042590085-2.

Despite the variety of methods of LiNbO<sub>3</sub> waveguide fabrication the need to obtain ever higher operational parameters of integrated optical chips for new applications, such as, for example, microfluidics [15], stimulates research into new technological processes and individual regimes. Also, the increasing production of such devices dictates research trends focused on the technological process time reduction, both by accelerating individual stages and by means of automation. One of the important practical problems of this study is the experimental efficiency confirmation of the high-speed etching of lithium niobate in fluorine-containing plasma with an increased consumption of plasma gases without forced thermostating of the sample.

However, the formation of waveguides is undoubtedly an important, but not the final task of forming an integrated optical chip. To interact with other chips or fiber elements of optoelectronic circuits, they must be coupled with special Optical Fibers (OF). There are quite a few requirements for such a coupling: firstly, the maximum optical power must be injected into the integrated optical chip; secondly, such a connection should have minimal reflections; thirdly, the process should be automated, as efficient as possible and fast. We propose to use the frequency domain reflectometry method for this [16]. Data obtained with the backscattering method is presumably optimum for fine alignment.

The methodology described in this work can become the basis for a series of technological experiments to optimize the technologies for the production of integrated-optical chips. We are starting now from plasma-chemical formation regimes of ridge waveguides, this stage's first results were also briefly reported in Russian in a local journal [17].

## II. PLASMA-CHEMICAL ETCHING OF LITHIUM NIOBATE

Lithium niobate, due to its unique physical properties, is widely used in photonics, functional electronics and microsystem technology. In particular, integrated-optical circuits based on lithium niobate are widely used in fiber-optic communication lines as modulators, optical switches and elements of wavelength division multiplexing systems [18]. Methods for creating diffuse waveguides in lithium niobate have been widely used, but recently there is the problem of creating on the surface of lithium niobate various ridge waveguides with high contrast and thin films within the framework of the lithium niobate-on-insulator technology [19]. The development of a technology for creating ridge waveguides based on lithium niobate will improve the characteristics of radiation modulators for fiber-optic communication lines, as well as expand the scope of its application by the development of integrated-optical erbium amplifiers and terahertz optics devices [20], [21].

In addition, the use of lithium niobate can be significantly expanded with microfluidics and the creation of full-fledged laboratories on a chip, which implies the integration of microfluidic channels, optical waveguides, and optoelectronic devices on a single chip

[22]. The potential for the use of lithium niobate in microfluidic technologies is due to its extensive use in integrated optics, the possibility of creating microfluidic pumps on its surface using the technology of surface acoustic wave generation, as well as its high biological, chemical resistance and other features [23], [24].

The main difficulty in creating ridge waveguides [25] and other microrelief structures in lithium niobate is the problem of its dimensional machining, due to its high chemical resistance, mechanical hardness and high fragility.

One of the promising methods for creating a microrelief on the surface of lithium niobate is plasma-chemical etching in a fluorine-containing plasma. The references describes attempts to etch lithium niobate in the discharges CF<sub>4</sub> [9], CHF<sub>3</sub> [10], C<sub>3</sub>F<sub>8</sub> [11], and SF<sub>6</sub> [12], as well as their mixtures with Ar and O<sub>2</sub>. However, the stable production of deep microstructures (~100 μm) with a high aspect ratio, low surface roughness and a sufficient etching rate has not yet been achieved. In addition, the results of etching obtained by different scientific groups at different setups and technological processes, different crystallographic sections of a crystal by different manufacturers are often impossible to repeat, due to a very large list of influencing factors.

The aim of this part is to supplement the practical experience in the problem of plasma-chemical etching of lithium niobate using the ETNA-100-PT-1 setup (Fig. 1). The key installation parameters: Two radio frequency (RF=13.56 MHz) generators with 600 and 300 watts maximum power, for inductively coupled plasma (ICP) and Capacitively Coupled Plasma (CCP) respectively. The ICP electrode diameter is 103 mm. The distance between the ICP electrode and the stage with the sample is about 100 mm. Working pressure in the reactor chamber 10<sup>-4</sup> ÷ 10<sup>-1</sup> mbar. Etching unevenness over the sample area less than 5%.

In particular, the study of etching the Y-cut of lithium niobate in a gas mixture of SF<sub>6</sub> and Ar with an increased volumetric flow rate and the simultaneous use of two plasma sources: An inductively coupled plasma (ICP) source and a capacitively coupled plasma (CCP) source. The choice of the gas mixture is due with a focus on the relevant studies [26], [27].

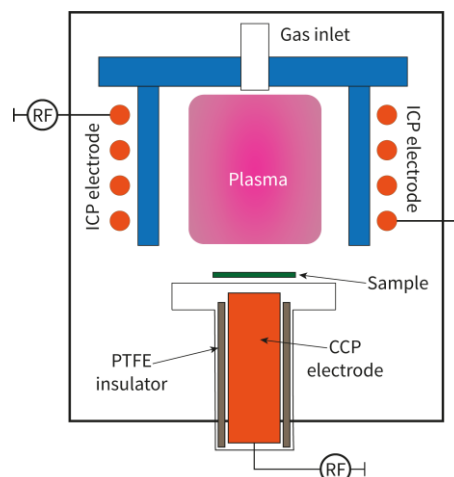


Fig. 1. The plasma etching setup ETNA-100-PT-1.

The experiment was carried out with ETNA-100-PT-1 setup equipped with two plasma discharge sources with the possibility of their simultaneous use. As a sample, we used a Y-cut of a lithium niobate crystal 2×1.5 cm in size, which were cut with a circular saw from an industrially produced wafer. Etching was performed with the simultaneous use of CCP and ICP plasma sources in a mixture of SF<sub>6</sub> and Ar gases. Although in most works was noted that the etching rate strongly depends on the temperature set on the sample substrate [26], [27], thermostating of the substrate holder was not performed, because an increase in the sample temperature leads to a decrease of the etching anisotropy and may lead to sample destruction [27]. Instead of thermostating the sample, a flat CCP electrode built into the sample holder was used (Fig. 1). Due to a voltage of several hundred volts between the surface of the flat electrode and the grounded chamber, positively charged ions and free radicals are captured by the rapidly changing field and vibrate around the substrate, forming a static electric field.

Preliminary experiments with a volumetric flow rate of gases equal to 50 mg/ml for SF<sub>6</sub> and Ar for each gas with a total pressure about 10 Pa showed that a layer with a thickness less than 500 nm was etched out within 30 minutes. This indirectly confirms the fact that at a relatively high pressure (more than 5 Pa), the mean free path of chemically active particles is not long enough to achieve sufficient etching rates.

To carry out the target experiment, Table I listed the selected etching parameters.

TABLE I: PLASMA ETCHING PARAMETERS

Parameter	Value	Units
Inductively coupled plasma power, $W_{ICP}$	500	W
Capacitively-coupled plasma power, $W_{CCP}$	200	W
Time of one etching step, $t$	10	min
Chamber pressure, $p$	2	Pa
Gas volumetric flow SF <sub>6</sub>	20	ml/min
Gas volumetric flow Ar	10	ml/min

The peculiarities of the experiment were the increased volumetric flow rates of SF<sub>6</sub> and Ar gases, while maintaining a relatively low pressure in the reaction chamber and the simultaneous use of two plasma sources. It should be noted separately that at the first stage of etching, a lithium niobate plate was placed between the substrate holder and the sample under study, which is supposed to provide a decrease in the temperature gradient and contribute to a more uniform distribution of plasma inside the chamber.

A targeted experiment to determine the etching rate was carried out in several stages:

1. Cleaning the sample in argon plasma for 1 minute to remove organic traces contaminating.
2. Weighing a sample on an analytical balance CAS CAUW 200D to determine the initial sample mass  $m_0$ .
3. Etching of a sample for 10 minutes with a volumetric flow rate of SF<sub>6</sub>= 20 mg/ml, Ar = 10 mg/ml and a pressure of 2 Pa.

4. Cleaning the sample in a 40% solution of hydrofluoric acid for 30 seconds in order to remove the non-volatile compound LiF, formed as a result of the interaction of sulfur hexafluoride with the sample surface [26], [27].
5. Re-weighing the sample and determining the etched mass of the sample.
6. Repeated etching of the sample for 10 minutes with a volumetric flow rate of SF<sub>6</sub> = 20 mg/ml, Ar = 10 mg/ml and a pressure of 2 Pa.
7. Sample cleaning in 40% hydrofluoric acid solution for 30 seconds.
8. Weighing the sample and determining the removed mass.

Further, the surface and the cleaved end face of the etched sample and a similar sample cut from the same wafer were examined using an electron microscope and an attachment for energy dispersive analysis in order to determine the etching structure and the presence of fluorine compounds in the surface layer.

The interest in the research of a sample cleaved end face arose due to the fact that it was demonstrated the defective near-surface layer, the presence and features of the structure of which can directly affect the etching results [28].

As a result of the experiment, at the first etching iteration, a high etching rate of the crystal surface layer was achieved even in the absence of forced heating of the substrate holder, which was ~930 nm/min (Table II).

TABLE II: FIRST ETCHING STEP RESULTS

Initial sample mass (g)	Sample mass after etching and removal of the LiF layer (g)	Mass variation (g)	Etched layer thickness (μm)	Etching rate (nm/min)
0.70870	0.69580	0.01290	9.3478	934,78

It should be noted that all experiments were carried out in rooms of ISO class 7 of cleanliness. The sample mass was measured at each stage several times, the measurement error did not exceed  $5 \cdot 10^{-5}$  grams.

The upper plane of the sample after the first stage of etching was covered with a light brown layer similar to that described in [26] and [27], which was easily removed with a napkin. The surface under this layer was mat white, indicating a successful etching process. The surface of the sample near the edges (about 0.5 mm from each edge) is more matte, which indicates that the sample is etched near the edges a little faster than in the center. An examination with an optical microscope showed that the difference in the height of the sample after etching from the edge to the center is not more than 1 μm. The lower surface of the sample remained glossy. Note that after the first stage of etching, the lithium niobate plate placed between the substrate holder and the sample was destroyed as a result of the temperature gradient; thus, the second stage of etching was carried out without it.

At the second step, the etching cycle was repeated without changing the parameters, except for the presence of a substrate in the chamber. The result of measuring the removed mass of lithium niobate is shown in Table III.

TABLE III: SECOND ETCHING STEP RESULTS

Initial sample mass (g)	Sample mass after etching and removal of the LiF layer (g)	Mass variation (g)	Etched layer thickness ( $\mu\text{m}$ )	Etching rate (nm/min)
0.69580	0.69222	0.00358	2.5990	259.90

It must be noted that at the second stage of etching, the rate of the process decreased by almost 4 times, but it still remained quite high. It is proposed that such a significant change in the etching rate can be caused by two factors. Firstly, by the influence of a defective near-surface layer present in industrial wafers [28]. It is assumed that at the first stage of etching, the defect layer was removed at an increased rate, and then the undamaged surface was etched more slowly. Secondly, the possible effect on reaction acceleration produced by a lithium niobate substrate in the reaction chamber, however, remains unclear and requires extra studies.

To test this hypothesis, at the next stage, using a scanning electron microscope (SEM), we studied the freshly cleaved faces end of the samples: the original wafer and the etched sample (Fig. 2).

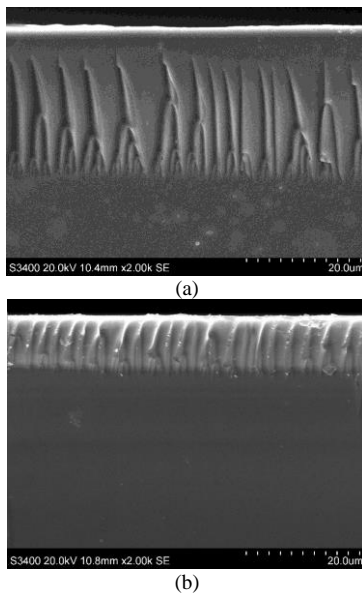


Fig. 2. SEM images of the cleaved end faces of the samples: (a) initial sample and (b) sample after plasma-chemical etching.

In the cleaved end face image of the original sample, there is a defect layer with a thickness of about  $20\ \mu\text{m}$  (Fig. 2(a)), described in [28]. The thickness of the defect layer after etching has decreased significantly - by about 10 microns (Fig. 2(b)), which satisfactorily correlates with the results of the substance removed mass measuring. Also, the fracture of the near-surface layer after etching is conchoidal and is depicted in much more contrast. This effect indicates an increase of the near-surface layer defectiveness and the possible emergence of a larger number of dislocations on the crystal surface, as a result of which, the metal, that is deposited before the electron microscopic examination of any dielectrics, concentrates on these defects and increases the conductivity and, as a consequence, the image contrast. However, the complete removal of the defective layer did not occur. Thus, the hypothesis that the defective layer was removed at the

first stage of etching, and then the rate of the etching of the intact layer turned out to be lower, was not confirmed. However, this does not mean that the reaction deceleration mechanism is not associated with the depth inhomogeneity of the crystal plate. It is possible that the part of the defect layer close to the surface has a different fine structure, which critically affects the rate of its etching. For a detailed understanding of the effect of the surface layer structure of lithium niobate on the rate of its plasma-chemical etching, additional research is required.

In addition to the end faces, SEM was also used to study the surfaces of the etched sample and a similar sample from the same wafer. The SEM images show that the original sample surface has no microstructure and is rather smooth on a scale of a few microns. The etched sample surface is covered with etching defects, and these defects are combined into clusters and present on the entire surface, which confirms the transition of the process to the active etching phase (Fig. 3).

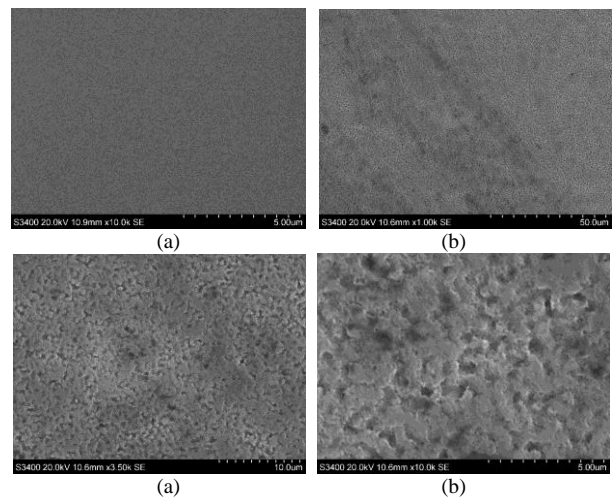


Fig. 3. SEM photo of the surface before and after plasma chemical etching: (a) initial sample surface ( $\times 10000$ ), (b) sample surface after two etching steps ( $\times 1000$ ), (c) sample surface after two etching steps ( $\times 3500$ ), and (d) sample surface after two etching steps ( $\times 10000$ ).

The SEM images show that the original sample surface has no microstructure and is rather smooth at a scale of a few microns. The etched sample surface is covered with etching defects, and these defects are combined into clusters and present on the entire surface, which confirms the transition of the process to the active etching phase. Further, different surface parts were analyzed by energy dispersive analysis for the content of fluorine compounds near the surface. The presence of fluorine's significant amount of was not detected, so this means that the samples treatment in a 40% solution of hydrofluoric acid for 30 seconds after plasma-chemical etching made it possible to completely remove non-volatile fluorine compounds.

The demonstrated characteristics of the process generally indicate its potential suitability for the formation of ridge waveguides. Its regimes will be varied many times, until the optimal parameters are reached. Meanwhile, continuing these iterative processes, we took several samples of integrated-optical chips with already formed waveguides in order to work out their coupling with OF.

### III. OPTICAL FIBER INTERFACING WITH WAVEGUIDES

Optical interfacing is the process of input and output of optical radiation from an external element into the waveguides of an integrated optical chip by creating an inseparable connection with an external element. Such elements can be OF, semiconductor laser diodes, photodiodes, lenses, and other chips. In this paper, an interfacing with an OF is considered. The optical interfacing consists of two parts: alignment and the resulting connection fixation with soldering, laser microwelding or gluing [29]. This part of work is devoted to alignment.

The relative position of the channel waveguide and the OF is determined by their lateral, longitudinal and angular displacements [30]. Alignment is used to adjust the OF and the waveguide. It is carried out using manipulators that control the spatial movement and orientation of the OF or the chip. Despite the fact that both the OF and the chip can move during the alignment, in practice the chip is most often in a stationary position. The manipulator system has six degrees of freedom: three spatial coordinates  $X, Y, Z$  and three angles  $\theta_x, \theta_y, \theta_z$  (Fig. 4).

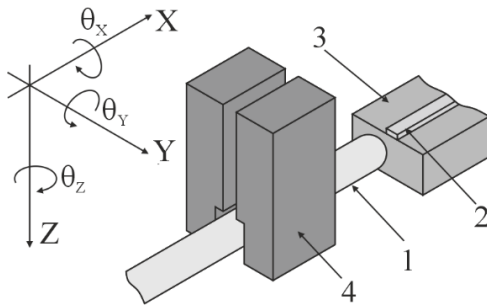


Fig. 4. Waveguide and OF alignment. 1 – optical fiber; 2 – channel waveguide; 3 – integrated optical chip; 4 – manipulators system, providing the movement of the optical fiber along three coordinates  $X, Y, Z$  and three angles  $\theta_x, \theta_y,$  and  $\theta_z$ .

Depending on the magnitude of the displacements between the OF and the waveguide, the alignment can be divided into coarse and fine. Coarse alignment is performed when the OF and the waveguide are displaced relative to each other so that it is not possible to input or output an optical signal. This alignment can be performed by preliminary injection of visible radiation into the waveguide [31]. However, this method is laborious and difficult to automate. Methods based on computer vision, such as [32], are quite well-known. But these techniques have strict requirements for the appearance of the objects being adjusted and are poorly applicable in laboratory conditions, where the samples under study have slightly different sizes. In this work, to perform the coarse alignment, we used the alignment technique based on the waveguide far end reflections using the method of Optical Frequency Domain Reflectometry (OFDR), presented in [33]. The technique was chosen on the basis of the following: it does not have strict requirements for the size and shape of the samples; allows an independent injection of optical signal into the waveguide for each of the end faces and an ease for automation. For the implementation of the coarse alignment, a setup from [33]

was used. In contrast to [33], here the alignment was performed not until the OFDR-trace maximum, corresponding to the far end of the waveguide, is reached, but only until the partial appearance of this peak. This approach made it possible to perform the initial adjustment less accurately, but much faster. Then fine adjustment can be applied.

Fine alignment uses the transmitted optical signal as feedback. Appealing to the mathematics, fine adjustment is a multidimensional optimization problem. The objective function is the level of the optical signal output from the waveguide of the integrated optical chip. The objective function should be maximized.

The most common methods used for fine alignment are: the hill climbing method, the Nelder-Mead method, the steepest descent method, and the genetic algorithm [34]–[37]. These methods are well researched but have a number of disadvantages. The hill climbing method has a low rate of convergence, since it does not take into account the direction of the objective function increase. The Nelder-Mead method has a low convergence rate, converges poorly near the maximum and in the presence of plateaus and ridges in the objective function. The steepest descent method converges poorly in the vicinity of the maximum of the objective function. The genetic algorithm has a low convergence rate and requires careful selection of parameters. To overcome the disadvantages of existing methods, a modification of the Newton's method with a descent direction was used (Fig. 5).

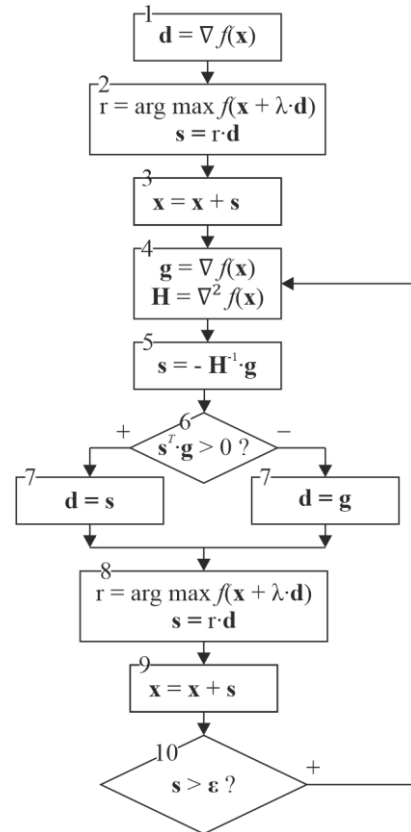


Fig. 5. Flowchart of the modified Newton's method:  $\mathbf{d}$  - search direction,  $\mathbf{x} = (y, z)$  - set of coordinates along axes  $Y$  and  $Z$  (Fig. 4),  $f(\mathbf{x})$  - objective function,  $\mathbf{r}$  and  $\lambda$  - one-dimensional optimization speed parameters,  $\mathbf{g}$  - gradient,  $\mathbf{H}$  - Hessian matrix,  $\mathbf{s}$  - direction found by the Newton's method.

The main idea of the classical Newton's method is to iteratively use the quadratic approximation of the objective function at the current search point and maximize this approximation. Hence the classical Newton's method is not effective far from the objective function maximum. The modified Newton's method starts with one iteration of the steepest descent method. At the Step 1, the gradient  $\nabla f(\mathbf{x})$  is calculated:

$$\nabla f(\mathbf{x}) = \left[ \frac{f(\delta, 0) - f(-\delta, 0)}{2\delta} \quad \frac{f(0, \delta) - f(0, -\delta)}{2\delta} \right]^T \quad (1)$$

$$\mathbf{H} = \begin{bmatrix} \frac{f(\delta, 0) - 2f(0, 0) + f(-\delta, 0)}{\delta^2} & \frac{f(\delta, \delta) - f(\delta, 0) - f(0, \delta) + f(0, 0)}{\delta^2} \\ \frac{f(\delta, \delta) - f(\delta, 0) - f(0, \delta) + f(0, 0)}{\delta^2} & \frac{f(0, \delta) - 2f(0, 0) + f(0, -\delta)}{\delta^2} \end{bmatrix} \quad (2)$$

At the Step 5, the vector  $\mathbf{s}$  was determined, indicating the direction of the objective function growth. In contrast to the classical Newton's method, if the condition at the Step 6 was not met, then the  $\mathbf{s}$  was not taken as the direction of the objective function increase. In this case, the direction of the increase was taken as the direction of the gradient  $\mathbf{g}$  and iteration was performed using the steepest descent method 7. Otherwise, the iteration was performed by the Newton's method 7. At the Step 8 and Step 9, along the direction selected in the Step 7 a one-dimensional optimization is performed and a new position of the OF  $\mathbf{x}$  is found.

At the Step 10, the adjustment was stopped at the moment when, in order to move to a new position, according to Step 9, it was necessary to perform a step having a value below the minimum step manipulator  $\boldsymbol{\varepsilon} = (\varepsilon, \varepsilon)$ .

The peculiarity of the modified Newton's method is that the steepest descent is performed where it is most effective - far from the maximum, and Newton's method begins to be executed when approaching the maximum, i.e. where the steepest descent loses its effectiveness. In this case, since at the beginning the fiber is most often located far from the waveguide, the first iteration is always performed with the steepest descent.

To assess the efficiency of alignment of the waveguide and OF using the modified Newton's method, the number of iterations spent on alignment was compared with the classical Newton's method, the steepest descent method and the hill climbing method. To search for nearby points, as well as to determine the gradient and the Hessian matrix, manipulator step  $\boldsymbol{\delta} = (0.5, 0.5) \mu\text{m}$  was used. The alignment was stopped at the moment when the subsequent displacement did not exceed  $\boldsymbol{\varepsilon} = (0.2, 0.2) \mu\text{m}$  along the Y axe and Z axe. A channel waveguide with a mode field diameter of  $\sim 7 \mu\text{m}$  and an OF with a mode field diameter of  $\sim 8 \mu\text{m}$  along Y axe and Z axe was adjusted. Under similar conditions, the modified Newton's method reached the objective function maximum in 5 iterations, while the steepest descent method in 8 iterations, the classical Newton's method in 9 iterations and the hill climbing method in 14 iterations (Fig. 6). Taking into account that the time spent in one

where  $\boldsymbol{\delta} = (\delta, \delta)$  is manipulator step size along axe Y and axe Z (Fig. 4).

At the Step 2 and Step 3, along the direction of the gradient a one-dimensional optimization is performed and a new position of the OF  $\mathbf{x}$  is found.

At the Step 4, the gradient  $\mathbf{g}$  and the Hessian matrix  $\mathbf{H}$  of the objective function  $f(\mathbf{x})$  were calculated. The gradient  $\mathbf{g}$  was calculated by (1). The calculation of the Hessian matrix was carried out according to (2).

iteration by the modified Newton's method was about 1.2 times the time of the steepest descent iteration, the modified Newton's method performed the adjustment 25% faster than the steepest descent.

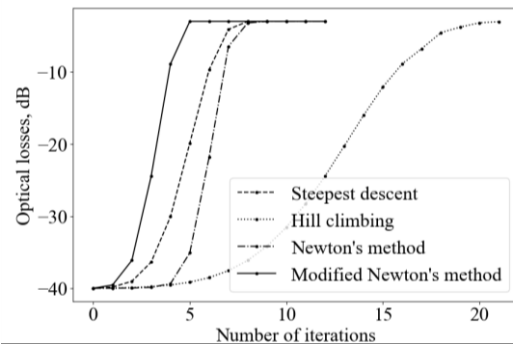


Fig. 6. Comparative characteristic of waveguide and optical fiber alignment with the steepest descent method, hill climbing method, Newton's method and modified Newton's method.

#### IV. RESULTS DISCUSSION AND PERSPECTIVES

As a result of the study, the possibility of achieving high etching rates of lithium niobate (up to 950 nm/min) in fluorine-containing plasma with an increased consumption of plasma-forming gases without forced thermostating of the sample was demonstrated. Using SEM, structural changes in the surface have been demonstrated: clustering of surface etching defects, indicating the uniformity of etching at the macroscale, and changes in the thickness and structure of the near-surface defect layer, indicating the possibility of its complete removal by the plasma-chemical method.

The results obtained confirm the prospects of research in the field of plasma-chemical treatment of lithium niobate and can be used to create a relief on the surface of lithium niobate, for example, ridge waveguides, microdisk resonators, and microfluidic channels.

It is expected that the upcoming research work will be dedicated to the acquisition of statistically significant results, as well as to a separate study of the various factors influence on the rate and quality of surface etching. In particular, the influence of the lithium niobate plate disposition between the sample and the substrate

holder. It is also planned to conduct experiments on the creation of ridge waveguides and microfluidic channels on lithium niobate using plasma-chemical etching.

Regarding the interfacing of the integrated-optical chip with the fiber optic guide, the presented combination of the alignment technique based on reflections from the far end face of the waveguide and fine alignment using the modified Newton's method allow: first, to simplify the alignment process by performing coarse alignment based on reflections from the far end face of the waveguide; secondly, to speed up the alignment process by using the modified Newton's method during fine alignment; third, to fully automate the alignment of the waveguide and OF at any initial displacements. In the course of further work, the limitations of the presented methods application will be studied thoroughly.

In general, the effect of the simultaneous practical application of both process improvements remains to be investigated. To do this, it is first necessary to collect broader empirical data for each of the stages described in this work. Then, within the framework of research in an industrial laboratory, evaluate changes in the economic and operational characteristics of the product.

#### CONFLICT OF INTEREST

The authors declare no conflict of interest.

#### AUTHOR CONTRIBUTIONS

M.E. Belokrylov, A.A. Kozlov, R.S. Ponomarev conducted the experiment in Unit II. P. V. Karnaushkin conducted the experiment in Unit III, Yu.A. Konstantinov implemented the scientific supervision, A. T. Turov assisted with the experiments and carried out paper composition.

#### ACKNOWLEDGMENT

The authors are grateful to Shustov D.O. for preparing the experimental samples. The Unit II study was funded by RFBR, project № 20-32-90186, the Unit III study was funded by state assignment № AAAA-A19-119042590085-2.

#### REFERENCES

- [1] E. J. Murphy, *Integrated Optical Circuits and Components: Design and Applications*, CRC press, 2020, pp. 10-43
- [2] R. Ponomarev, Y. Konstantinov, M. Belokrylov, *et al.*, "Reflectometry study of the pyroelectric effect on proton-exchange channel waveguides in lithium niobate," *Applied Sciences*, vol. 11, no. 21, 2021.
- [3] H. Hu, R. Ricken, and W. Sohler, "Low-loss ridge waveguides on lithium niobate fabricated by local diffusion doping with titanium," *Applied Physics B*, vol. 98, no. 4, pp. 677-679, 2010.
- [4] E. L. Wooten, K. M. Kissa, A. Yi-Yan, *et al.* "A review of lithium niobate modulators for fiber-optic communications systems," *IEEE Journal of Selected Topics in Quantum Electronics*, vol. 6, no. 1, pp. 69-82, 2000.
- [5] S. M. Kostitsky, Y. N. Korkishko, V. A. Fedorov, *et al.* "Subsurface disorder and electro-optical properties of proton-exchanged LiNbO<sub>3</sub> waveguides produced by different techniques," *Journal of the European Optical Society: Rapid Publications*, vol. 9, 2014.
- [6] J. H. Zhao, X. H. Liu, Q. Huang, *et al.*, "Lithium niobate ridge waveguides fabricated by ion implantation followed by ion beam etching" *Journal of Lightwave Technology*, vol. 28, no. 13, pp. 1913-1916, 2010.
- [7] L. Gui, B. Xu, and T. C. Chong, "Microstructure in lithium niobate by use of focused femtosecond laser pulses," *IEEE Photonics Technology Letters*, vol. 16, no. 5, pp. 1337-1339, 2004.
- [8] D. Brüske, S. Sunstov, C. E. Rüter, *et al.*, "Efficient ridge waveguide amplifiers and lasers in Er-doped lithium niobate by optical grade dicing and three-side Er and Ti in-diffusion," *Optics Express*, vol. 25, no. 23, pp. 29374-29379, 2017.
- [9] W. Sun, X. Yang, R. Piao, *et al.*, "Z-propagation Ti: Er: Tm: LiNbO<sub>3</sub> strip waveguide with Er<sup>3+</sup>/Tm<sup>3+</sup> codoped," *Proc. of SPIE*, vol. 10339, 2017.
- [10] M. Neradovskiy, H. Tronche, D. Chezganov, *et al.*, "Nonlinear characterization of waveguide index profile: Application to soft-proton-exchange in LiNbO<sub>3</sub>," *Journal of Lightwave Technology*, vol. 39, no. 14, pp. 4695-4699, 2021.
- [11] B. Zhang, L. Wang, and F. Chen, "Recent advances in femtosecond laser processing of LiNbO<sub>3</sub> crystals for photonic applications," *Laser & Photonics Reviews*, vol. 14, no. 8, 2020.
- [12] L. G. Carpenter, S. A. Berry, and C. B. E. Gawith, "Ductile dicing of LiNbO<sub>3</sub> ridge waveguide facets to achieve 0.29 nm surface roughness in single process step," *Electronics Letters*, vol. 53, no. 25, pp. 1672-1674, 2017.
- [13] L. Cai, A. Mahmoud, and G. Piazza, "Low-loss waveguides on Y-cut thin film lithium niobate: towards acousto-optic applications," *Optics Express*, vol. 27, no. 7, pp. 9794-9802, 2019.
- [14] C. Shen, C. Wang, Y. Zhu, *et al.*, "A comparative study of dry-etching nanophotonic devices on a LiNbO<sub>3</sub>-on-insulator material platform," *Proc. of SPIE*, vol. 11781, 2021.
- [15] J. Mei and J. Friend, "A review: Controlling the propagation of surface acoustic waves via waveguides for potential use in acoustofluidics," *Mechanical Engineering Reviews*, vol. 7, no. 1, pp. 19-00402, 2020.
- [16] F. L. Barkov, Yu. A. Konstantinov, S. D. Bochkova, *et al.*, "Modelling of polarised optical frequency domain reflectometry of axially twisted anisotropic optical fibres," *Quantum Electronics*, vol. 49, no. 5, pp. 514-517, 2019.
- [17] M. E. Belokrylov, A. A. Kozlov, and Yu. A. Konstantinov "Features of plasmochemical etching lithium niobate for creation of integral optical modulators with ridge waveguide," *LAST MILE Russia*, 2021 (in Russian, paper accepted, in print).
- [18] J. L. Kwang, L. Sheng, F. Parmigiani, I. Morten, *et al.*, "OTDM to WDM format conversion based on quadratic cascading in a periodically poled lithium niobate waveguide," *Opt. Express*, vol. 18, no. 10, pp. 10282-10288, 2010.
- [19] S. Siew, E. Cheung, H. Liang, A. Bettiol, N. Toyoda, B. Alshehri, E. Dogheche, and A. Danner, "Ultra-low loss ridge waveguides on lithium niobate via argon ion milling and gas clustered ion beam smoothening," *Opt. Express*, vol. 26, no. 4, pp. 4421-4430, 2018.
- [20] S. Toroghi, J. Rollinson, M. Hella, I. Wilke, and P. Rabiei, "Thin film lithium niobate optical modulators for THz frequency applications," *Proc. SPIE*, vol. 11279, 2020.
- [21] M. Zhukova, M. Melnik, I. Vorontsova, A. Tsytkin, *et al.*, "Estimations of low-inertia cubic nonlinearity featured by electro-optical crystals in the THz range," *Photonics*, vol. 7, no. 4, p. 98, 2020.
- [22] G. Bettella, R. Zamboni, G. Pozza, A. Zaltron, C. Montecocchi, *et al.*, "LiNbO<sub>3</sub> integrated system for opto-microfluidic sensing," *Sensors and Actuators B: Chemical*, vol. 282, pp. 391-398, Mar. 2019.
- [23] N. Jagatpal, A. Mercante, A. Ahmed, and D. Prather, "Thin film lithium niobate electro-optic modulator for 1064 nm wavelength," *IEEE Photonics Technology Letters*, vol. 33, no. 5, pp. 271-274, 2021.
- [24] K. Shima, N. Mitsugi, and H. Nagata, "Surface precipitates on single crystal LiNbO<sub>3</sub> after dry-etching by CHF<sub>3</sub> plasma," *Journal of Materials Research*, vol. 13, no. 3, pp. 527-529, 1998.
- [25] W. Park, W. Yang, W. Kim, *et al.*, "Ridge structure etching of LiNbO<sub>3</sub> crystal for optical waveguide applications," *Optical*

Materials, vol. 28, pp. 216-220, Feb. 2006.

- [26] V. V. Gulyaev., J. I. Dikerev, V. M. Rubinstein, S. M. Tsvetkov, and E. N. Bormontov, "High-rate plasma-chemical etching of lithium niobate," *Kondensirovannye Sredy I Mezhfaznye Granitsy = Condensed Matter and Interphases*, vol. 12, no. 4, pp. 360-368, 2010. (in Russian).
- [27] A. Osipov, A. Osipov, G. Iankevich, A. Speshilova, *et al.*, "Deep etching of LiNbO<sub>3</sub> using inductively coupled plasma in SF<sub>6</sub>-based gas mixture," *Journal of Microelectromechanical Systems*, vol. 30, no. 1, pp. 90-95, 2021.
- [28] A. Sosunov, R. Ponomarev, S. Mushinsky, A. Volyntsev, *et al.*, "Effect of the structure of the lithium niobate surface layer on the characteristics of optical waveguides," *Crystallography Reports*, vol. 65, no. 5, pp. 786-791, 2020.
- [29] S. Siala, "Method and apparatus for coupling an optical fiber to an optoelectronic device," *Oesys Photonics, Inc. Pat. US US6174092B1*, 1999.
- [30] H. C. Lefevre, "Fiber optic gyroscope," in *Fiber-Optic Sensors, J. Dakin and B. Culshaw, Eds.*, Norwood, MA: Artech House, 1989.
- [31] R. P. Nonhebel and B. P. J. Stienen. (2013). Alignment in Integrated Optical Systems. [Online]. Available: <http://purl.utwente.nl/essays/63389>.
- [32] Y. Zheng and B. Xia, "High precision fast line detection of alignment and coupling for planar optical waveguide device," *Optik*, vol. 145, pp. 519-528, 2017.
- [33] P. Karnaushkin and Y. Konstantinov, "An experimental technique for aligning a channel optical waveguide with an optical fiber based on reflections," *Instruments and Experimental Techniques*, vol. 64, no. 5, pp. 709-714, 2021.
- [34] Z. Tang, F. Zhang, and F. Shi, "Effects of angular misalignments on fiber-optic alignment automation," *Optics Communications*, vol. 196, pp. 173-180, Sept. 2001.
- [35] C. Fuh, Y. Hsu, R. Li, and H. Tsai, "Simplex method applied in the fiber-optic alignment," in *Proc. Research for Int. Conf.*, 2017, pp. 20-21.
- [36] M. Yu, T. Lin, Y. Li, and P. Shu, "A study on the optimization methods for optomechanical alignment," *Proceedings of SPIE*, vol. 6289, 2006.
- [37] H. Nosato, M. Murakawa, and T. Higuchi, "Automatic alignment of multiple optical components using genetic algorithm," in *Proc. First NASA/ESA Conference on Adaptive Hardware and Systems*, 2006, pp. 67-73.

Copyright © 2022 by the authors. This is an open access article distributed under the Creative Commons Attribution License ([CC BY-NC-ND 4.0](https://creativecommons.org/licenses/by-nc-nd/4.0/)), which permits use, distribution and reproduction in any medium, provided that the article is properly cited, the use is non-commercial and no modifications or adaptations are made.



**Maxim E. Belokrylov** was born in 1993, Perm region/Russia. He received the specialist diploma in solid state physics from the PSU in 2015. Now he is working in UB RAS Laboratory of Agriophotonics as a junior researcher and he is a postgraduate student of Department of Nanotechnology and Microsystem Technology. Research interests: fiber lasers, reflectometry, plasma etching, integrated optics, biosensors.



**Andrey A. Kozlov** received the master's diploma in Nanotechnology and Microsystem Technology from the Perm State National Research University in 2018. Now he is a postgraduate student and assistant of the Nanotechnology and Microsystem Technology department. Research interests: photonic integrated circuits, technologies for creating waveguide structures.



**Pavel V. Karnaushkin** was born in 1993. He received the diploma degree in solid state physics from the Perm State National Research University in 2016. Now he is working in Photonics Laboratory UB RAS as a junior researcher. Research interests: integrated optics, assembly and packaging of integrated optical devices, optoelectronics.



**Yuri A. Konstantinov**, Ph.D., Born 1984. 2006 - graduated from the Electrical Engineering Faculty of the PSTU. 2012 – Ph.D. degree in technical sciences. 2013 – present – Senior Researcher of the Photonics Laboratory of the Perm Federal Research Center of the Ural Branch of the RAS. Research interests: automated non-destructive methods for studying fiber optics elements, distributed fiber optic sensors



**Roman S. Ponomarev** was born in Perm/Russia in April, 1987. He received the diploma degree in solid state physics from the Perm State University, Perm/Russia in 2009 and Ph.D. in photonics (2014). Now he is head of integrated photonics lab in Perm University and senior researcher in Photonics Lab of PFRC UB RAS. Research interests include fabrication and characterization of optical waveguides in ferroelectrics, optical modulators and biosensors.



**Artem T. Turov** received Bachelors in photonics and optical informatics from ITMO University in 2020 and currently pursuing Master Degree at Department of general physics, Perm National Research Polytechnic University. In addition, he works as an engineer in UB RAS agriophotonics lab. His area of interest includes terahertz holography and imaging techniques, numerical simulation, fiber optic DAS and optical reflectometry sensors.